

Simultaneous multifrequency radio observations of the Galactic Centre magnetar SGR J1745–2900

P. Torne,^{1*} R. P. Eatough,¹ R. Karuppusamy,¹ M. Kramer,^{1,2} G. Paubert,³
B. Klein,^{1,4} G. Desvignes,¹ D. J. Champion,¹ H. Wiesemeyer,¹ C. Kramer,³
L. G. Spitler,¹ C. Thum,³ R. Güsten,¹ K. F. Schuster,⁵ and I. Cognard^{6,7}

¹Max-Planck-Institut für Radioastronomie, Auf dem Hügel 69, D-53121, Bonn, Germany

²Jodrell Bank Centre for Astrophysics, School of Physics and Astronomy, The University of Manchester, Manchester M13 9PL, UK

³Instituto de Radioastronomía Milimétrica, Avda. Divina Pastora 7, Núcleo Central, 18012, Granada, Spain

⁴Hochschule Bonn-Rhein-Sieg, Grantham-Allee 20, D-53757, Sankt Augustin, Germany

⁵Institut de Radioastronomie Millimétrique, 300 rue de la Piscine, F-38406, Saint Martin d'Hères, France

⁶Laboratoire de Physique et Chimie de l'Environnement et de l'Espace CNRS-Université d'Orléans, F-45071, Orléans, France

⁷Station de radioastronomie de Nançay, Observatoire de Paris, CNRS/INSU, F-18330, Nançay, France

Accepted 2015 April 22. Received 2015 April 16; in original form 2015 March 21

ABSTRACT

We report on simultaneous observations of the magnetar SGR J1745–2900 at frequencies $\nu = 2.54$ to 225 GHz using the Nançay 94-m equivalent, Effelsberg 100-m, and IRAM 30-m radio telescopes. We detect SGR J1745–2900 up to 225 GHz, the highest radio frequency detection of pulsed emission from a neutron star to date. Strong single pulses are also observed from 4.85 up to 154 GHz. At the millimetre band we see significant flux density and spectral index variabilities on time scales of tens of minutes, plus variability between days at all frequencies. Additionally, SGR J1745–2900 was observed at a different epoch at frequencies $\nu = 296$ to 472 GHz using the APEX 12-m radio telescope, with no detections. Over the period MJD 56859.83 – 56862.93 the fitted spectrum yields a spectral index of $\langle\alpha\rangle = -0.4 \pm 0.1$ for a reference flux density $\langle S_{154} \rangle = 1.1 \pm 0.2$ mJy (with $S_\nu \propto \nu^\alpha$), a flat spectrum alike those of the other radio-loud magnetars. These results show that strongly magnetized neutron stars can be effective radio emitters at frequencies notably higher to what was previously known and that pulsar searches in the Galactic Centre are possible in the millimetre band.

Key words: stars: neutron – pulsars: general – pulsars: individual: SGR J1745–2900 – stars: magnetars – Galaxy: centre – radiation mechanisms: non-thermal

1 INTRODUCTION

Magnetars are thought to be neutron stars with extremely strong magnetic fields (Duncan & Thompson 1992). Further work by Thompson & Duncan (1995, 1996) theorized how the decay of the strong magnetic fields in magnetars can produce soft gamma-ray and X-ray emission and proposed that Anomalous X-ray Pulsars (AXPs) and Soft Gamma Repeaters (SGRs) could indeed be magnetars. This identification of AXPs and SGRs as magnetars was validated when pulsations with spin-down (a typical characteristic of pulsars) were first detected from one of these objects (Kouveliotou et al. 1998). At the time of writing, 23 magnetars have been discovered (for a review, see Olausen & Kaspi 2014), and only four have conclusively shown pulsed radio emis-

sion (Camilo et al. 2006, 2007a; Levin et al. 2010; Eatough et al. 2013; Shannon & Johnston 2013). SGR J1745–2900, the subject of this work, is the last one discovered, and is a compelling object due to its proximity to Sagittarius A* (Sgr A*), the supermassive black hole candidate in the Galactic Centre (GC). Initially discovered at high energies (Kennea et al. 2013; Mori et al. 2013; Rea et al. 2013), pulsations in the radio band up to 20 GHz were also detected with different radio telescopes (Eatough et al. 2013; Shannon & Johnston 2013).

One peculiar characteristic of radio-loud magnetars is that they tend to show shallower spectral indices than ordinary pulsars. This property makes magnetars unique sources to obtain pulsar observations at high radio frequencies, where ordinary pulsars are, with a few exceptions (Kramer et al. 1997b; Morris et al. 1997; Löhmer et al. 2008), usually too faint to be detected and studied. This underexplored re-

* E-mail: ptorne@mpifr-bonn.mpg.de

gion of the spectrum of emission is valuable in the study of pulsar emission physics. For instance some emission models include effects that may only be detectable at high radio frequencies, like “coherence breakdown” between the radio and infrared bands where an incoherent component of emission becomes dominant (Michel 1982). Additionally, unexpected effects have been seen in some of the high frequency pulsar observations available to date: spectral flattening (Kramer et al. 1996), variability in flux density (Kramer et al. 1997a) or changes in polarization degree (Xilouris et al. 1996).

This particular source lies in the vicinity of Sgr A*. It has been shown that pulsars closely orbiting the black hole could be used to test General Relativity and alternative theories of gravity to the highest precision (Liu et al. 2012). Because the scattering towards the GC remains not well understood (Bower et al. 2014; Spitler et al. 2014), and scattering may still limit our chances of finding pulsars in the GC, SGR J1745–2900 is therefore a useful target for tests of high-frequency observations of the GC.

We present here observations of the magnetar SGR J1745–2900 from 2.54 to 472 GHz. Section 2 describes the observations and data reduction. Our results are presented in Section 3. Finally, a summary and discussion are given in Section 4.

2 OBSERVATIONS AND DATA REDUCTION

Nançay and Effelsberg: At the Nançay radio telescope, observations were taken at a central frequency of 2.54 GHz with a bandwidth of 512 MHz. Data from dual linear polarizations were coherently dedispersed, folded modulo the magnetar period and recorded to disc. The observations were flux density calibrated using the standard PSRCHIVE¹ software routines that require the use of a calibrated noise diode in combination with observations of a calibration source; in this case 3C286 was used. Observations at 4.85 and 8.35 GHz were made at the Effelsberg 100-m radio telescope using both a digital spectrometer, operating in a pulsar search mode, and a coherent dedispersion system. At each frequency dual circular polarizations were recorded over a total bandwidth of 500 MHz. A calibrated noise diode was used to determine the flux density scale by comparing it to NGC7027. Data were processed with the SIGPROC² software package.

IRAM 30-m: Observations in the millimetre band were made at the IRAM 30-m radio telescope and used the Eight MIXer Receiver (EMIR, Carter et al. 2012) with the Broad-Band-Continuum (BBC) backend. The BBC is connected to four outputs of EMIR working with dual frequency bands and dual sideband mixers. Two frequency combinations were used: centred at 87, 101, 138, 154 GHz (Mode E0/E1) and 87, 101, 209, 225 GHz (mode E0/E2). The effective bandwidth of the BBC is estimated to be 24 GHz (6 GHz per frequency band). Both horizontal (H) and vertical (V) linear polarizations were recorded. We noted a systematic lower sensitivity in the H polarization channel, the cause of which we were not able to identify. A special set-up of the backend enabled fast time sampling of the continuum signal

at 1 ms. The total variations of the system temperature (T_{sys}) during the four days were between 77–183 K for the 87 GHz band, 84–208 K for the 101 GHz band, 87–257 K for 138 GHz band, 98–327 K for the 154 GHz band, 478–571 K for the 209 GHz band and 520–621 K for the 225 GHz band. Temporal fluctuations in the atmospheric water vapour are responsible for the high variations of T_{sys} . We observed in “Total Power” mode, i.e. always on source. This observing mode has the disadvantage that atmospheric and receiver gain variations are reflected in the data as variations of the mean count level. Self-produced instrumental interference was present in the data, in particular at harmonics of 1 Hz, most likely produced by the cryogenerator.

The data reduction was as follows. The dispersion delay due to the interstellar medium, even at the large $\text{DM} = 1778 \text{ cm}^{-3} \text{ pc}$ of the source, is only $\Delta t_{\text{DM}} \simeq 0.9 \text{ ms}$ across the observing frequency range. This delay is smaller than the sampling time of 1 ms and therefore negligible. The variations in the time series and interference needed to be removed because they contaminated significantly the baseline of the folded pulsar profile, reducing our sensitivity to the pulsed emission. Our solution consisted of using a sliding window of width 3 s where a sine wave of 1 Hz and baseline were fit to the data, subtracting the central 1 s of the fit from the raw data. This reduced the variations enough to produce a nearly flat-baseline folded profile. For 209 and 225 GHz, this method was less effective than a running mean filtering, that was applied twice to the time series with windows of 10 and 0.4 s, respectively. Both filtering methods subtract the continuum emission contribution from the GC. Finally, the cleaned time series were folded with the topocentric period of SGR J1745–2900, calculated from a recent ephemeris from a timing analysis performed at lower frequencies. The flux density calculations were done using interspersed hot-cold load calibration measurements at the beginning and end of each observation scan, providing the required quantities to convert counts to antenna temperature T_{a}^* . The methodology follows Kramer (1997). The conversion factor from T_{a}^* to flux density (S/T_{a}^*) was obtained from the observatory efficiency tables³. Pointing corrections were also applied between scans. In addition, due to the low telescope elevations during the observations, an elevation-dependent telescope-gain correction was applied (Peñalver 2012). Our flux density calibration method was verified with pointings on the planets Mars and Uranus.

APEX: Additional millimetre and submillimetre data were taken with the APEX radio telescope. The system used was the FLASH⁺ receiver with a special version of the continuum Pocket BackEnd (PBE). FLASH⁺ worked in dual sideband mode providing simultaneously four bands centred at 296, 308, 460, and 472 GHz. The total bandwidth was 16 GHz (4 GHz per frequency band), splitting and recording one polarization at 296 and 308 GHz and the other at 460 and 472 GHz. The sampling time of the continuum signal was 0.5 ms. SGR J1745–2900 was observed on 2014 August 24 for 60 min. T_{sys} varied during the observation between 119–130 K for the 296 GHz band, 129–143 K for the 308 GHz band, 589–811 K for the 460 GHz band, and 471–3414 K for the 472 GHz band. The atmospheric water

¹ <http://psrchive.sourceforge.net/>

² <http://sigproc.sourceforge.net/>

³ <http://www.iram.es/IRAMES/mainWiki/Iram30mEfficiencies>

vapour content is responsible for the high T_{sys} at 460 and 472 GHz. Again, “Total Power” measurements were done. We applied the two-running-mean method with 10 and 0.4 s windows to reduce the variations in the time series and subtract the continuum contributions of the atmosphere and GC. The cleaned time series were then folded using the topocentric period of SGR J1745–2900 computed from our ephemeris. For the non-detection flux density limits, the radiometer equation with a signal-to-noise threshold of 5, duty cycle of 0.075, and telescope gain from the observatory efficiency tables⁴ is used (see e.g. Lorimer & Kramer 2005). Factors to account for the transmissivity of the atmosphere are also included.

Within the constraints of the source visibility the observations from IRAM 30-m, Effelsberg and Nançay were simultaneous, overlapping a total of 203 min on the dates 2014 July 22–24. Table 1 summarizes the observations.

3 RESULTS

The magnetar was clearly detected up to 154 GHz and more weakly detected at 209 and 225 GHz with clear peaks at the expected rotational phase. At APEX, 296 to 472 GHz, no detections were made. Fig. 1 shows the detected average profiles at each frequency. The profiles are generally multi-component, with a shape that varied significantly from day to day at the lowest frequencies 2.54 to 8.35 GHz. At the millimetre band the profile was more stable, showing a main peak and a precursor (pulse phase $\simeq 0.15$ in Fig. 1). The precursor seems to consist of different narrow components that appeared and disappeared randomly between observations, and was on average stronger at the highest frequencies.

In Table 1 we present the equivalent continuum flux density (also known as the “mean flux density”) from all observations. The errors were estimated taking into account the uncertainties in the calibration processes. We observed significant variations in flux density on short time-scales (of the order of tens of minutes) in the millimetre data and day-to-day variability at all frequencies. Fig. 2 shows the total averaged mean flux density per frequency band and a power-law fit to the data spanning more than 220 GHz. Over the period MJD 56859.83 – 56862.93 the fitted spectrum yields a spectral index of $\langle\alpha\rangle = -0.4 \pm 0.1$ for a flux density at 154 GHz $\langle S_{154} \rangle = 1.1 \pm 0.2$ mJy.

We also detected numerous single pulses at all frequencies between 4.85 and 154 GHz (at 2.54 GHz the delivered folded data did not allow to search for single pulses). At the millimetre band, the peak flux density of the strongest pulses reached 19 Jy at 101 GHz, with a pulse width of 1 ms. Following Lorimer & Kramer (2005), this is equivalent to a brightness temperature $T_B > 10^{23}$ K, for a distance to the GC of 8.3 kpc (Gillissen et al 2009). At 154 GHz, the strongest pulse reached a peak of 8 Jy with a width of 1 ms and $T_B \simeq 2.3 \cdot 10^{22}$ K. The majority of the single pulses detected showed T_B of the order of 10^{22} K. The values calculated here are lower limits because we are limited by the coarse time resolution of the data. Fig. 3 shows a selection of strong single pulses from our data set at the highest

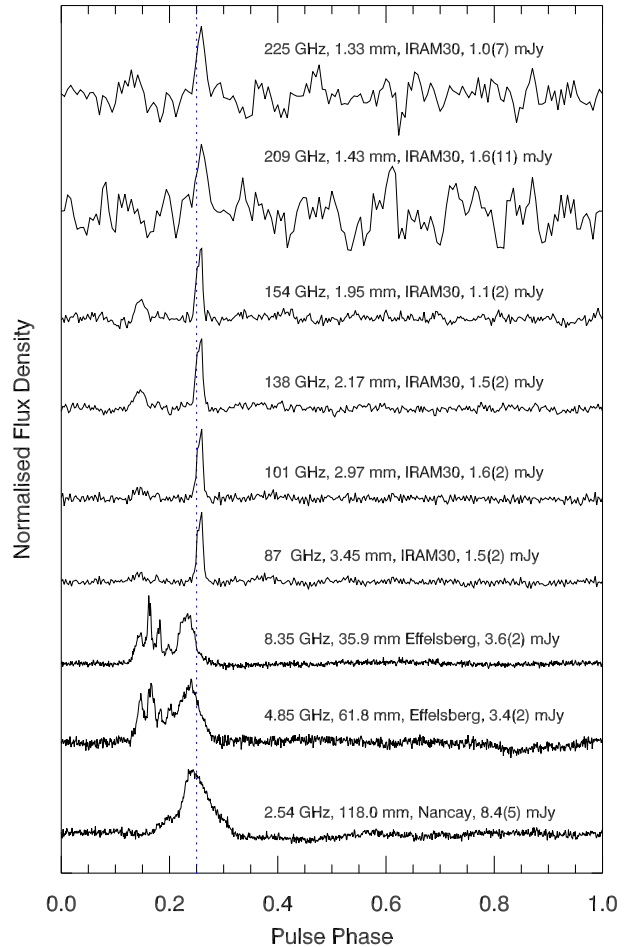


Figure 1. Average pulse profiles of SGR J1745–2900 at 2.54, 4.85, 8.35, 87, 101, 138, 154, 209 and 225 GHz. All profiles are generated from the sum of the observations presented here and are aligned to the same reference phase obtained from our timing ephemeris (dotted line).

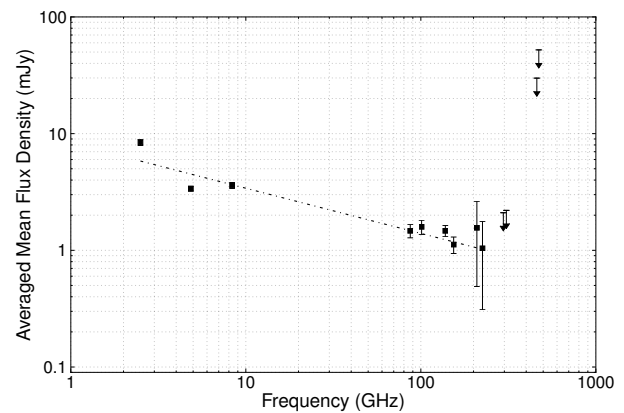


Figure 2. Total averaged mean flux densities. The dash-dotted line shows the spectral index fit. The mean spectral index obtained for SGR J1745–2900 is $\langle\alpha\rangle = -0.4 \pm 0.1$, showing the unusual flatter spectrum common to magnetars in the radio band. Due to the variability of the source the APEX data (taken approximately one month later) were not used to prove or disprove the continuation of the power law beyond 230 GHz.

⁴ <http://www.apex-telescope.org/telescope/efficiency/index.php>

Table 1. Summary of the observations of SGR J1745–2900 with measured flux densities and spectral indices. For July 21 the relative error bars are too large for a meaningful spectral index fit. Note that the APEX observations are one month later from the rest. In the observatory column, (Obs.) I corresponds to IRAM30-m, N to Nançay, E to Effelsberg and A to APEX. Errors in the last digits are shown in parenthesis.

Date	Obs.	ν (GHz)	S (mJy)	α	T_{obs} (h)
2014 Jul 21	I	87	0.1(4)	–	2.0
		101	0.6(5)		2.0
		138	0.2(3)		2.0
		154	0.3(4)		2.0
2014 Jul 22	N	2.54	10.5(11)	–0.3(1)	1.3
		4.85	3.9(3)		1.0
		8.35	3.3(3)		0.8
	I	87	1.5(3)		4.0
		101	1.8(3)		4.0
		138	2.2(3)		4.0
		154	1.5(3)		4.0
2014 Jul 23	N	2.54	11.0(11)	–0.4(1)	1.3
		4.85	4.0(3)		1.1
		8.35	3.3(3)		1.1
	I	87	1.8(4)		2.4
		101	1.7(5)		2.4
		138	1.7(3)		2.4
		154	1.9(4)		2.4
2014 Jul 24	N	2.54	3.8(4)	–0.2(1)	1.3
		4.85	2.2(3)		1.1
		8.35	4.2(4)		1.1
	I	87	2.6(4)		2.0
		101	2.1(4)		2.0
		138	0.8(4)		0.8
		154	0.6(5)		0.8
2014 Aug 24	A	209	1.6(11)	–	1.2
		225	1.0(7)		1.2
		296	< 2.1		1.0
		308	< 2.2		1.0
		460	< 29.9		1.0
Total average	N	2.54	8.4(5)	–0.4(1)	3.9
		4.85	3.4(2)		3.1
		8.35	3.6(2)		3.0
	I	87	1.5(2)		10.4
		101	1.6(2)		10.4
		138	1.5(2)		9.2
		154	1.1(2)		9.2
		209	1.6(11)		1.2
		225	1.0(7)		1.2

frequencies. A detailed analysis of the single pulses from SGR J1745–2900 will be presented elsewhere.

Possible reasons for the non-detections at APEX include the comparably lower sensitivity of the observations, the faintness of the source at these frequencies, and the random variability of the source. We also noted strong, periodic self-produced instrumental interference overlapping the magnetar spin frequency that could have decreased our sensitivity even further. The polarization splitting of the APEX receiver (see §2), if the magnetar is highly linearly polarized at these frequencies, could have also led to a loss in sensitivity if the radiation was misaligned with the feed at the

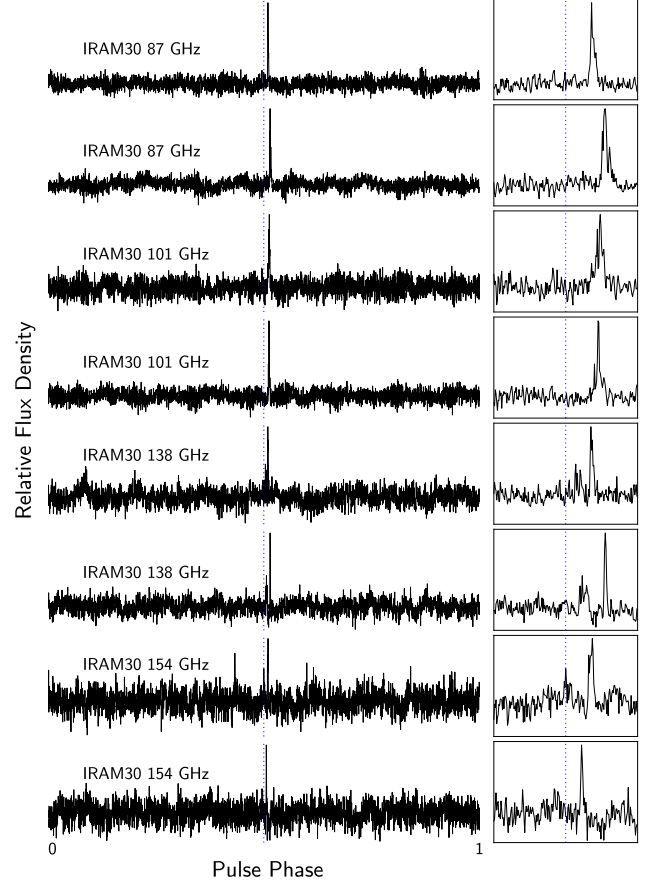


Figure 3. Selection of strong single pulses from our data set in the millimetre band. The time resolution is 1 ms. The panels on the left show one rotation of the neutron star. Panels on the right show a zoom to a window of 0.2 s around the reference phase computed from the ephemeris (dotted line). The width, intensity and morphology of the single pulses are diverse. The features visible in the off-pulse region are due to residual interference.

lower bands, 296 and 308 GHz, that were much more sensitive. Because of these uncertainties, we cannot conclusively rule out the emission of SGR J1745–2900 between 296 and 472 GHz, nor a lack of it.

4 SUMMARY AND DISCUSSION

The detections of SGR J1745–2900 up to 225 GHz and its single pulses up to 154 GHz set new records for the detection of pulsed emission from a neutron star in the radio band. The high measured flux density of SGR J1745–2900 at the millimetre band between 87 and 225 GHz, $\langle S_{\text{mm}} \rangle = 1.4 \pm 0.2$ mJy, and the numerous strong single-pulses detected up to 154 GHz show that SGR J1745–2900 can be, at least during some periods of activity, an efficient producer of radiation at very high radio frequencies. In combination with the work by Camilo et al. (2007b), our detections suggest that emission at very high radio frequencies from radio-loud magnetars might be a frequent characteristic of these objects.

The origin of the radio emission from magnetars is still

unclear. The case of magnetars is perhaps more complex than for ordinary pulsars, which are thought to be powered entirely by their loss of rotational kinetic energy, (also called “spin-down luminosity”) \dot{E} . Some magnetars show luminosities at high energies that are much larger than \dot{E} (see, e.g., Tables 2 and 7 in Olausen & Kaspi 2014), requiring additional sources to power their electromagnetic emission. Big efforts have been made trying to model processes that describe the emission from magnetars (Thompson & Duncan 1995; Beloborodov & Thompson 2007; Beloborodov 2009, 2013), but the puzzle is not yet solved. From our observations, we can infer some properties of the radio emission from SGR J1745–2900. For the high brightness temperatures of the single pulses, $T_B \sim [10^{22} - 10^{23}]$ K, a coherent mechanism for the radio emission is required. Following Lorimer & Kramer (2005), its radio luminosity is estimated to be $R_{\text{lum}} \sim 10^{29} \text{ erg s}^{-1}$, assuming a duty cycle of 0.15 and an emission cone opening angle of 4° . Its spin-down luminosity is $\dot{E} \sim [10^{33} - 10^{34}] \text{ erg s}^{-1}$, depending on what timing solution is used (our own, or e.g. Kaspi et al. 2014; Lynch et al. 2014). Therefore, $R_{\text{lum}}/\dot{E} \sim [10^{-4} - 10^{-5}]$. This shows that the radio emission could be powered by its rotational kinetic energy; although this does not mean that this is the source or rule out that other mechanisms are involved. SGR J1745–2900 shows common characteristics with ordinary pulsars, and remarkable differences, like it is for the other three known radio magnetars (Kramer et al. 2007; Camilo et al. 2008; Lazaridis et al. 2008; Levin et al. 2012). The reason for this, as well as the details of the radio emission from pulsars in general, is still unknown.

Finally, the detection of SGR J1745–2900 up to 225 GHz at a distance of 8.3 kpc shows that it is, in principle, possible to search for pulsars in the GC at these frequencies. A key advantage of pulsar searches at millimetre wavelengths is that any deleterious effects caused by the GC interstellar medium (i.e. pulse scattering and dispersion) can be fully neglected. Along the same lines, any deleterious effects caused by the intergalactic medium, which are not well known, could also be neglected or will have a minimal impact. It might therefore also be an option to search for shallow-spectrum pulsars in nearby galaxies through single-pulse emission. At 1.4 GHz, the magnetar is more luminous than 97 per cent of all known pulsars, and it is by far the most luminous in the millimetre band. This fact alone suggests a larger less-luminous population that can be detected with increased sensitivity at the millimetre band. In any case, pulsar searches with more sensitive millimetre telescopes, such as ALMA, are promising.

ACKNOWLEDGEMENTS

We are grateful to the referee S. Johnston for very useful comments, to A. Jessner and D. Riquelme for discussions, to P. Lazarus for sharing code, and to C. Ng for reading the manuscript. Partly based on observations with the 100-m telescope of the MPIfR at Effelsberg. The Nançay radio observatory is operated by the Paris Observatory, associated to the French CNRS. IRAM is supported by INSU/CNRS (France), MPG (Germany) and IGN (Spain). APEX is a collaboration between the MPIfR, the European Southern Observatory, and the Onsala Space Observatory. PT is supported for this research through a stipend from the Interna-

tional Max Planck Research School (IMPRS) for Astronomy and Astrophysics at the Universities of Bonn and Cologne.

REFERENCES

- Beloborodov A. M., 2009, *ApJ*, 703, 1044
- Beloborodov A. M., 2013, *ApJ*, 777, 114
- Beloborodov A. M., Thompson C., 2007, *ApJ*, 657, 967
- Bower G. C. et al., 2014, *ApJ*, 780, L2
- Camilo F., Ransom S. M., Halpern J. P., Reynolds J., Helfand D. J., Zimmerman N., Sarkissian J., 2006, *Nature*, 442, 892
- Camilo F., Ransom S. M., Halpern J. P., Reynolds J., 2007a, *ApJ*, 666, L93
- Camilo F. et al., 2007b, *ApJ*, 669, 561
- Camilo F., Reynolds J., Johnston S., Halpern J. P., Ransom S. M., 2008, *ApJ*, 679, 681
- Carter M. et al., 2012, *A&A*, 538, A89
- Duncan R. C., Thompson C., 1992, *ApJ*, 392, L9
- Eatough R. P. et al., 2013, *Nature*, 501, 391
- Gillessen S., Eisenhauer F., Trippe S., Alexander T., Genzel R., Martins F., Ott T., 2009, *ApJ*, 692, 1075
- Kaspi V. M. et al., 2014, *ApJ*, 786, 84
- Kennea J. A. et al., 2013, *ApJ*, 770, L24
- Kouveliotou C. et al., 1998, *Nature*, 393, 235
- Kramer C., 1997, IRAM Internal Technical Memo
- Kramer M., Xilouris K. M., Jessner A., Wielebinski R., Timofeev M., 1996, *A&A*, 306, 867
- Kramer M., Xilouris K. M., Rickett B., 1997a, *A&A*, 321, 513
- Kramer M., Jessner A., Doroshenko O., Wielebinski R., 1997b, *ApJ*, 488, 364
- Kramer M., Stappers B. W., Jessner A., Lyne A. G., Jordan C. A., 2007, *MNRAS*, 377, 107
- Lazaridis K., Jessner A., Kramer M., Stappers B. W., Lyne A. G., Jordan C. A., Serylak M., Zensus J. A., 2008, *MNRAS*, 390, 839
- Levin L. et al., 2010, *ApJ*, 721, L33
- Levin L. et al., 2012, *MNRAS*, 422, 2489
- Liu K., Wex N., Kramer M., Cordes J. M., Lazio T. J. W., 2012, *ApJ*, 747, 1
- Löhmer O., Jessner A., Kramer M., Wielebinski R., Maron O., 2008, *A&A*, 480, 623
- Lorimer D. R., Kramer M., 2005, *Handbook of Pulsar Astronomy*, Cambridge University Press, Cambridge, UK
- Lynch R. S., Archibald R. F., Kaspi V. M., Scholz P., 2014, preprint (arXiv:1412.0610)
- Michel F. C., 1982, *Reviews of Modern Physics*, 54, 1
- Mori K. et al., 2013, *ApJ*, 770, L23
- Morris D. et al., 1997, *A&A*, 322, L17
- Olausen S. A., Kaspi V. M., 2014, *ApJS*, 212, 6
- Peñalver J., 2012, IRAM Internal Technical Memo
- Rea N. et al., 2013, *ApJ*, 775, L34
- Shannon R. M., Johnston S., 2013, *MNRAS*, 435, L29
- Spitler L. G. et al., 2014, *ApJ*, 780, L3
- Thompson C., Duncan R. C., 1995, *MNRAS*, 275, 255
- Thompson C., Duncan R. C., 1996, *ApJ*, 473, 322
- Xilouris K. M., Kramer M., Jessner A., Wielebinski R., Timofeev M., 1996, *A&A*, 309, 481